Cell Chemical Biology

De novo designed Hsp70 activator dissolves intracellular condensates

Graphical abstract

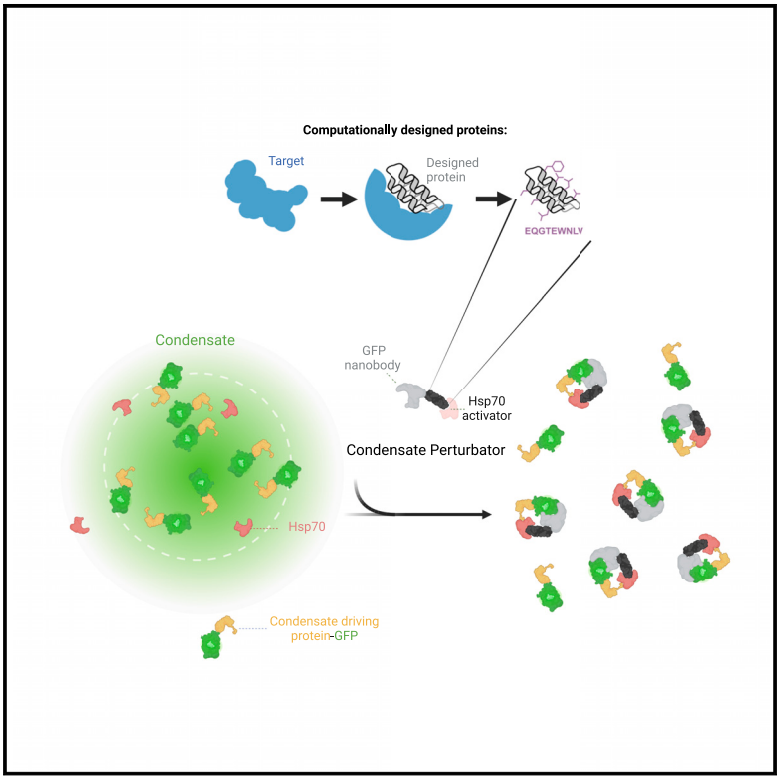

Highlights

- Computationally designed proteins modulate Hsp70 ATPase activity
- ATPase-stimulating designs enhance protein refolding, mimicking native co-chaperones
- Targeted designed proteins disrupt condensates revealing their cellular function

Authors

Jason Z. Zhang, Nathan Greenwood, Jason Hernandez, ..., Christine Queitsch, Jason E. Gestwicki, David Baker

Correspondence

jzz0428@uw.edu (J.Z.Z.), dabaker@uw.edu (D.B.)

In brief

Zhang et al. describe computationally designed proteins that modulate Hsp70 ATPase activity. One of these designs refolds proteins, dissolves intracellular condensates, and uncovers their cellular roles. This study advances our understanding of Hsp70-mediated protein quality control and offers new tools to regulate protein folding and cellular organization.

Zhang et al., 2025, Cell Chemical Biology *32*, 463–473
March 20, 2025 © 2025 University of Washington. Published by Elsevier Ltd.
https://doi.org/10.1016/j.chembiol.2025.01.006

CellPress

Cell Chemical Biology

CellPress
OPEN ACCESS

Technology

De novo designed Hsp70 activator dissolves intracellular condensates

Jason Z. Zhang,[1,2,3,8,*] Nathan Greenwood,[1,2] Jason Hernandez,[4,5] Josh T. Cuperus,[6] Buwei Huang,[1,2] Bryan D. Ryder,[4,5] Christine Queitsch,[6,7] Jason E. Gestwicki,[4,5] and David Baker[1,2,3,*]

[1]Department of Biochemistry, University of Washington, Seattle, WA 98195, USA
[2]Institute for Protein Design, University of Washington, Seattle, WA 98195, USA
[3]Howard Hughes Medical Institute, University of Washington, Seattle, WA 98195, USA
[4]Institute for Neurodegenerative Diseases, University of California, San Francisco, San Francisco, CA 94143, USA
[5]Department of Pharmaceutical Chemistry, University of California, San Francisco, San Francisco, CA 94143, USA
[6]Department of Genome Sciences, University of Washington, Seattle, WA 98195, USA
[7]Brotman Baty Institute for Precision Medicine, Seattle, WA 98195, USA
[8]Lead contact
*Correspondence: jzz0428@uw.edu (J.Z.Z.), dabaker@uw.edu (D.B.)
https://doi.org/10.1016/j.chembiol.2025.01.006

SIGNIFICANCE Cells constantly use and recycle their proteins in a process called protein quality control (PQC). Imbalance of PQC leads to accumulation of dysfunctional proteins, thus leading to a variety of diseases. Hsp70 is a central mediator of PQC by collaborating with J-domain proteins (JDPs) to regulate client protein folding and degradation. Despite the importance of this system, the molecular mechanisms governing these interactions remain unclear. This study employs computationally designed proteins to create synthetic Hsp70-binding proteins that can either enhance or inhibit its activity. One of these designs mimic native JDPs in promoting refolding of denatured proteins and can modulate intracellular condensates, revealing insights into the roles of these condensates. This work provides insight in three aspects: (1) computational and experimental methods to design synthetic binding proteins, (2) advances our understanding of Hsp70 interactions that regulate PQC, (3) introduces modular tools to manipulate Hsp70 activity and condensates. We anticipate that these results and tools will accelerate our understanding of PQC and manipulation of PQC in diseases.

SUMMARY

Protein quality control (PQC) is carried out in part by the chaperone Hsp70 in concert with adapters of the J-domain protein (JDP) family. The JDPs, also called Hsp40s, are thought to recruit Hsp70 into complexes with specific client proteins. However, the molecular principles regulating this process are not well understood. We describe the *de novo* design of Hsp70 binding proteins that either inhibit or stimulate Hsp70 ATPase activity. An ATPase stimulating design promoted the refolding of denatured luciferase *in vitro*, similar to native JDPs. Targeting of this design to intracellular condensates resulted in their nearly complete dissolution and revealed roles as cell growth promoting signaling hubs. The designs inform our understanding of chaperone structure-function relationships and provide a general and modular way to target PQC systems to regulate condensates and other cellular targets.

INTRODUCTION

Heat shock protein 70 (Hsp70) proteins are central components of protein quality control (PQC), playing roles in protein folding, trafficking, and turnover.[1] A key step in this process is Hsp70 recruitment to diverse "client" proteins by members of the J-domain protein (JDP) family of adapters.[2] The prototypical human JDP, DnaJA2, is composed of an N-terminal J-domain (JD), a glycine/phenylalanine (G/F)-rich region, two C-terminal domains (CTDI/II), and a dimerization motif. The JD is a conserved, four-helix bundle with a histidine-proline-aspartate (HPD) motif invariant across eukaryotes and prokaryotes.[3] The JD interacts with Hsp70 between the nucleotide binding domain (NBD) and the substrate-binding domain (SBD),[3] triggering large conformational

 © 2025 University of Washington. Published by Elsevier Ltd.
This is an open access article under the CC BY-NC-ND license (http://creativecommons.org/licenses/by-nc-nd/4.0/).

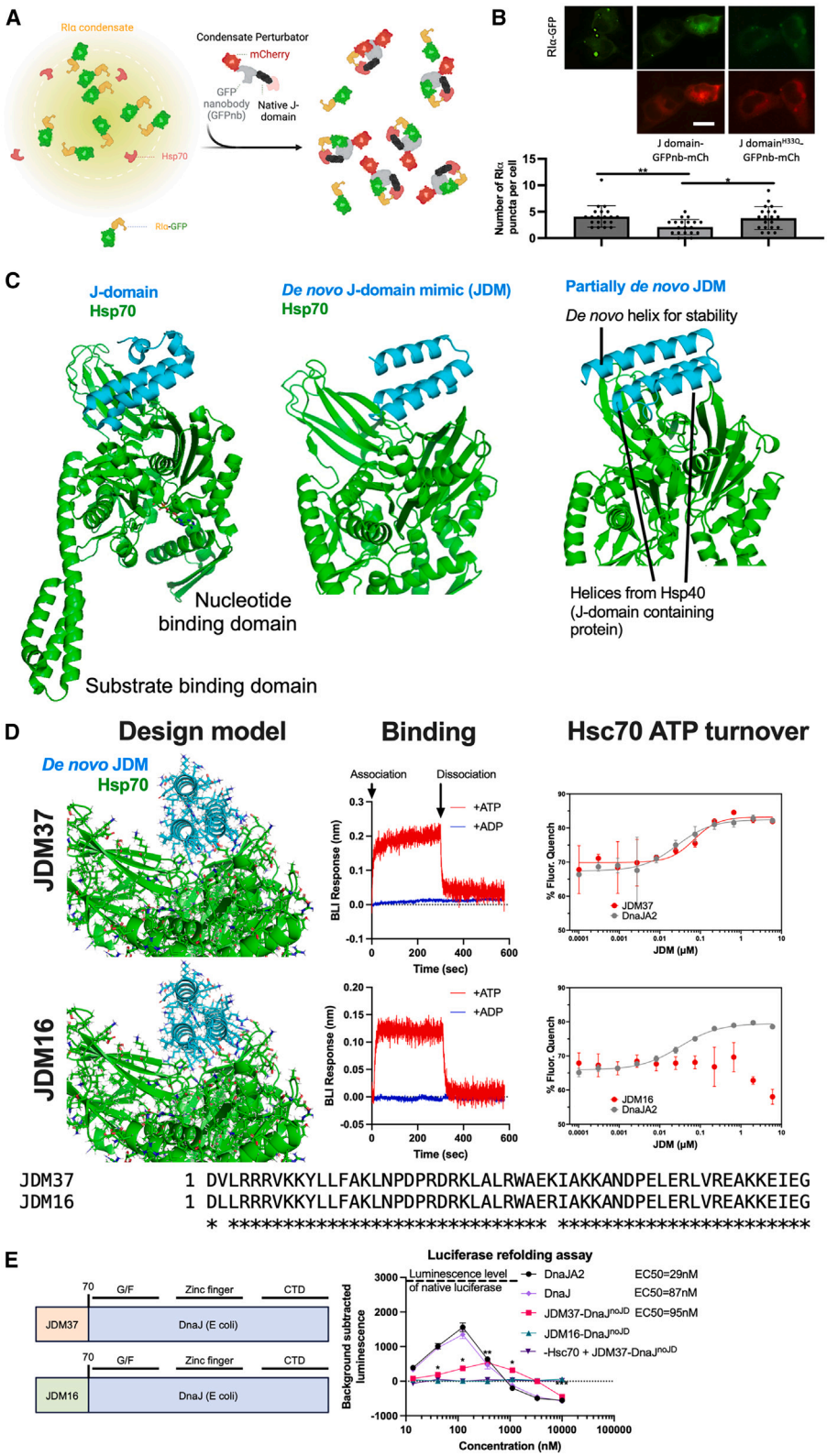

Figure 1. *De novo* design of Hsp70 binders/activators

(A) Experimental design. The driver of condensation (here, RIα) is fused with GFP. DnaJB1's JD is fused to a GFP nanobody (GFPnb) and mCherry (mCh), and this tool is called condensate perturbator.

(legend continued on next page)

changes in Hsp70 and accelerating Hsp70 ATPase activity. The CTDI/II domains interact with subsets of client proteins[4] to promote client "hand-off" to Hsp70.[5] Hsp70 clients are typically disordered protein domains, such as those involved in forming condensates, membrane-less intracellular structures that can selectively sequester biomolecules and are increasingly recognized for their numerous roles in shaping cell physiology. There are 45+ JDPs in humans and while some have been associated with specific functions,[6,7] it has proven challenging to ascertain the roles of many JDPs,[8,9] likely due to partial functional redundancies.

To gain molecular insights into the function of the natural PQC systems, and to enable targeting Hsp70 foldase activity to specific targets, we set out to *de novo* design modular, synthetic JDPs. Such synthetic proteins would need to specifically bind Hsp70, induce the conformational change and activate ATPase activity, and "hand-off" the client. As a test of the functional activity, we chose to use the effect of the designed JDPs on condensates, such as the physiologically relevant RIα condensates that are important for regulating cAMP/PKA signaling, because of their intrinsic importance and the simplicity of following them by fluorescence microscopy.

DESIGN

We first set out to determine whether recruiting Hsp70 via native JD is sufficient to dissolve condensates. As a previous study showed that DnaJB1 recruitment to RIα condensates can drastically reduce the number of RIα puncta,[2] we genetically fused the DnaJB1's JD to a GFP nanobody (GFPnb) and a mCherry (mCh) and transfected this "condensate perturbator" construct along with RIα tethered to GFP in HEK293T cells (Figure 1A). Maintaining similar expression for both constructs (Figures S1A and S1B), co-expression of this condensate perturbator with RIα-GFP led to decreases in the number of RIα puncta per cell and implementing the H33Q point mutation[10] in DnaJB1 JD, which disrupts Hsp70 binding, reverses the effect on RIα puncta numbers (Figure 1B). Local recruitment of Hsc70 (the human Hsp70) is required as simple overexpression of Hsc70 is insufficient to reduce RIα puncta numbers (Figure S1C). While the condensate perturbator using native JD reduces the number of RIα puncta, it did not completely eliminate them.

The native JD has a modest binding affinity for Hsp70 (kd∼500 nM). We reasoned that a tighter binder to Hsp70 could improve dissolution of the condensates, thus we set out to design *de novo* proteins which we call J-domain mimics (JDMs) that bind to Hsp70 at the same site as the native JD. We employed Rosetta protein design to construct JDMs in two ways (Figures 1C and S1D, see STAR Methods for details). First,[11] we designed fully *de novo* JDMs that are predicted to bind Hsp70 at the same site as native JDs but are unrelated in structure and sequence. Second,[12] we built upon the two helices within DnaJ (a well-studied *E. coli* JDP) that interact with its partner DnaK (the *E. coli* Hsp70) and added a third, designed helix to improve binding and monomer stability. In brief,[11] over a million designs were generated *in silico* and filtered based on their predicted binding to DnaK using Rosetta and AlphaFold2 (AF2) metrics (see STAR Methods for details). Although we intend to use these binders for Hsc70, high quality crystal structures of Hsp70:JDP interactions only exist for DnaK:DnaJ (PDB:5NRO)[13] and there is high sequence similarity for the JDP interaction site between DnaK and Hsc70 (Figure S1E). 20,000 of the fully *de novo* and 5,000 of the partially *de novo* JDM designs were displayed on the surface of yeast and sorted for binding to biotinylated Hsc70. From this screen, 4 fully *de novo* JDM designs bound to Hsc70, while none of the partially *de novo* JDMs did possibly due to the differences between *E. coli* DnaJ and human JDPs (Figure S1F). These four designs were then affinity matured through site-saturation mutagenesis (SSM) (Figures S1F and S1G) followed by combination of the positive variants into optimized JDMs. This process resulted in 41 JDM design variants that showed strong binding to immobilized Hsc70 at low concentration (10 nM). Like native JDs, the JDMs bound only to Hsc70 when bound to ATP, but not ADP, and they could be displaced by addition of a molar excess of a native JDP (human DnaJB1) (Figure S1H), suggesting that they bind the intended site.

RESULTS

Screening for active JDM designs

We purified the 41 JDMs from *E. coli* and measured their binding to Hsc70 by biolayer interferometry (BLI) (Figures S2 and S3). The designs had Hsc70 affinities ranging from 1 nM to 1 μM. Similar to native JDs, both the kon and koff of JDMs binding to Hsc70 were fast (kon: 1-9 × 10^5 M^{-1} s^{-1}, koff: 1-40 × 10^{-2} s^{-1}), which is likely important for Hsc70 processivity. In alignment with the yeast surface binding data (Figure S1H), the purified JDMs bound to Hsc70 in the ATP-bound state but not to the ADP-loaded Hsc70 (Figure 1D). Next, we investigated whether the designs could promote steady-state ATP turnover.

(B) Expression of condensate perturbators using native JD partially dissolves GFP-tagged RIα puncta in HEK293T cells. Top: representative epifluorescence images of the various conditions tested. Scale bar, 10 μm. Bottom: quantification of number of RIα puncta per cell. Each point represents a single cell (n = 20 cells). Statistics are two-way Student's t test. p values: *p < 0.05, **p < 0.01.

(C) Structure models of native and designed Hsp70 complexes. Left: crystal structure of DnaK (Hsp70) with DnaJ (Hsp40) (PDB: 5NRO). Middle: AlphaFold structure prediction of DnaK with fully *de novo* protein designed to bind to the same region as DnaJ. Right: AlphaFold structure prediction of DnaK with partially redesigned DnaJ.

(D) Design and biochemical characterization of fully *de novo* designed J-domain mimics (JDMs). Left: AlphaFold complex prediction of selected JDM with DnaK. Middle: representative trace of biolayer interferometry (BLI) measurements of JDM binding to either ATP or ADP-loaded Hsc70 (see STAR STAR Methods). Right: *in vitro* assays measuring ATP turnover by Hsc70 with either native DnaJA2 (Hsp40) or JDMs (see STAR Methods). Lines represent average of fluorescence quenching, which indicates ATP turnover (n = 3 experiments). Bottom: sequence alignment of the two JDMs presented here.

(E) *In vitro* assays measuring the refolding of denatured luciferase where Hsc70 and either native DnaJA2 (Hsp40), *E. coli* DnaJ, or JDM37 fused to DnaJ without its native J-domain (JDM37-$DnaJ^{no\ JD}$) was added (see STAR Methods). Lines represent average luminescence recorded (n = 3 experiments). Dotted line represents the average luminescence level of native luciferase. Statistics are two-way ANOVA. p values: *p < 0.05, **p < 0.01, ***p < 0.001. See also Figures S1–S6 and Table S1.

The 30 well expressing JDMs were tested at a range of concentrations for their ability to stimulate Hsc70 (1 μM) in ATP turnover assays (Figure S4A). While most inhibited Hsc70 ATP turnover, one of the designs, JDM37, promoted ATP hydrolysis, with EC_{50} and maximum turnover values comparable to DnaJA2 and isolated JD from DnaJA2 (Figures 1D and S4A). Designs which most competed with the ability of DnaJA2 to activate Hsc70 ATPase activity *in vitro* also suppressed *E. coli* growth at 42°C (Figure S5), suggesting that these designs block DnaJ:DnaK interactions in *E. coli*. In contrast, JDM37 expression in *E. coli.* led to the highest growth velocity (Figure S5B) possibly due to JDM37 activation of DnaK in *E. coli*, although this was not directly tested.

One of the competitive inhibitors, JDM16, differs in only two amino acids from the Hsc70 ATPase-inducing JDM37 design (Figure 1D); while JDM16 selectively interacts with ATP-loaded Hsc70, it does not induce ATP turnover (Figure 1D). Both substitutions were required for activity as constructs with one JDM16 residue and with one JDM37 residue at these two positions also did not lead to ATP hydrolysis (Figure S6H). Not surprisingly because of the subtlety of the changes, AlphaFold2 predictions of the interactions of the designs with Hsc70 (Figures S6A–S6C; Table S1) did not provide much insight into the mechanisms underlying JDM37-mediated Hsc70 ATPase activation. While there is very little sequence similarity between JDM37 and DnaJ, and JDM37 does not contain the highly conserved HPD motif, JDM37 and several inactivating designs do contain the sequence NPD motif which is structurally predicted to be positioned in the same area as the native HPD motif (Figures S6D–S6F). In addition, the electrostatics involved in Hsc70 binding (helices 2 for native J-domain and JDM37) are also largely conserved (Figure S6G) but cannot be the primary cause of Hsc70 activation as they are also present in the inactivating JDMs (Figure S2A).

The refolding of chemically denatured luciferase is a complex process that requires coordination of client hand-off during multiple cycles of ATPase activity.[14,15] This process requires not only the JD, but also the CTDI/II of natural JDPs.[16] Not surprisingly, we found that purified JDM37 alone does not promote Hsc70-mediated luciferase refolding (Figure S4B), as it lacks client binding activity. However, a chimera in which the natural JD of DnaJ is replaced by JDM37, together with Hsc70, did mediate luciferase refolding (Figure 1E). In contrast, replacing JDM37 with the inhibitor, JDM16, led to a chimera with no activity in luciferase refolding assay (Figure 1E). Thus, chimeras of *de novo* Hsp70 activators can recapitulate complex functions of JDPs. The Emax and EC_{50} for stimulation of luciferase refolding were 3-fold weaker for the chimera than for native Hsp40 (DnaJ and DnaJA2); this may reflect differences in ATP turnover, Hsc70 binding kinetics, or less efficient handoff of the client protein.

De novo JDM binds to and activates Hsp70 to dissolve intracellular condensates

With a higher affinity for Hsc70 (kd = 43.7 nM) than native JDs, we wondered if our *de novo* JDM that activated Hsc70 (JDM37) could more readily dissolve condensates than the native JD (Figures 1A and 1B). We explored the disruption of GFP containing condensates by a fusion of JDM37 to a GFP nanobody GFPnb[17] and mCh to follow localization (JDM37-GFPnb-mCh) (Figure 2A). Co-expression of this construct with GFP-tagged RIα in HEK293T cells led to nearly complete elimination of RIα puncta (Figures 2B and S7A–S7C). Expression of mCh tethered to GFPnb (GFPnb-mCh) alone or the Hsp70 inhibitor JDM16 tethered to GFPnb-mCh had no effect on number of RIα puncta per cell even though both JDM37 and JDM16 can bind to Hsc70 in cells (Figures 2C and S7D), suggesting that JDM-mediated condensate dissolution requires both binding and activation of Hsc70. Consistent with this, pharmacological inhibition of Hsp70 by VER-155008 reversed the elimination of RIα puncta by JDM37-GFPnb-mCh (Figure 2B), while VER-155008 itself did not increase total RIα puncta numbers as VER-155008 with GFPnb did not increase RIα puncta numbers compared to GFPnb alone (Figure 2B). Possible mechanisms for the reduction in RIα puncta are Hsp70-mediated degradation of client[18] or activation of the heat shock response, however RIα protein levels did not significantly differ across experimental conditions and heat shock responsive protein levels did not increase during expression of JDMs (Figures S7E and S7F), respectively. These results indicate that our *de novo* Hsp70 activator JDM37 can dissolve intracellular condensates by recruiting and locally activating Hsp70.

De novo JDM dissolves endogenous condensates

As protein expression levels can significantly affect condensate formation and biophysical properties, we next explored if JDM37 can dissolve endogenous condensates. To visualize proteins expressed at their endogenous levels, we used a set of HEK293T cell lines where the 11th β-strand of mNeonGreen[19] is inserted into the endogenous gene locus of coding proteins via CRISPR-Cas9 and the remaining β-strands of mNeonGreen are stably co-expressed, thus enabling reconstitution of a fluorescent GFP (Figure 3A). We focused on proteins (NONO, PSPC1, and SFPQ) that are critical for paraspeckle[20] formation, a naturally occurring condensate found in the nucleus that functions in regulating gene expression. In these cell lines (293-NONO, 293-PSPC1, and 293-SFPQ), we expressed our JDM37-GFPnb-mCh condensate perturbator construct and observed significant reduction of numbers of paraspeckles per cell, while expression of JDM16-GFPnb-mCh had no substantial effect (Figures 3B–3D and S8). These results were not due to depletion of paraspeckle protein as NONO, PSPC1, and SFPQ expression did not significantly change during JDM expression (Figures S8D, S8H, and S8L). Thus JDM37 can dissolve condensates formed at physiological expression levels.

Application of *de novo* JDM to investigate role of signaling condensates

There are few current tools to perturb condensates to assess their function. We used our JDM37-mediated condensate perturbator, to probe signaling roles of RIα condensates that sequester cAMP and active PKA to spatially compartmentalize their activity.[2] To visualize all at the same time the condensate perturbator, RIα, and fluorescent biosensors that measure cAMP/PKA signaling, RIα was tagged with mCherry (RIα-mCh) and JDM37 was fused with mCherry nanobody (mChnb)[17] and TSapphire (JDM37-mChnb-TSapphire) (Figure 4A). We found that expression of

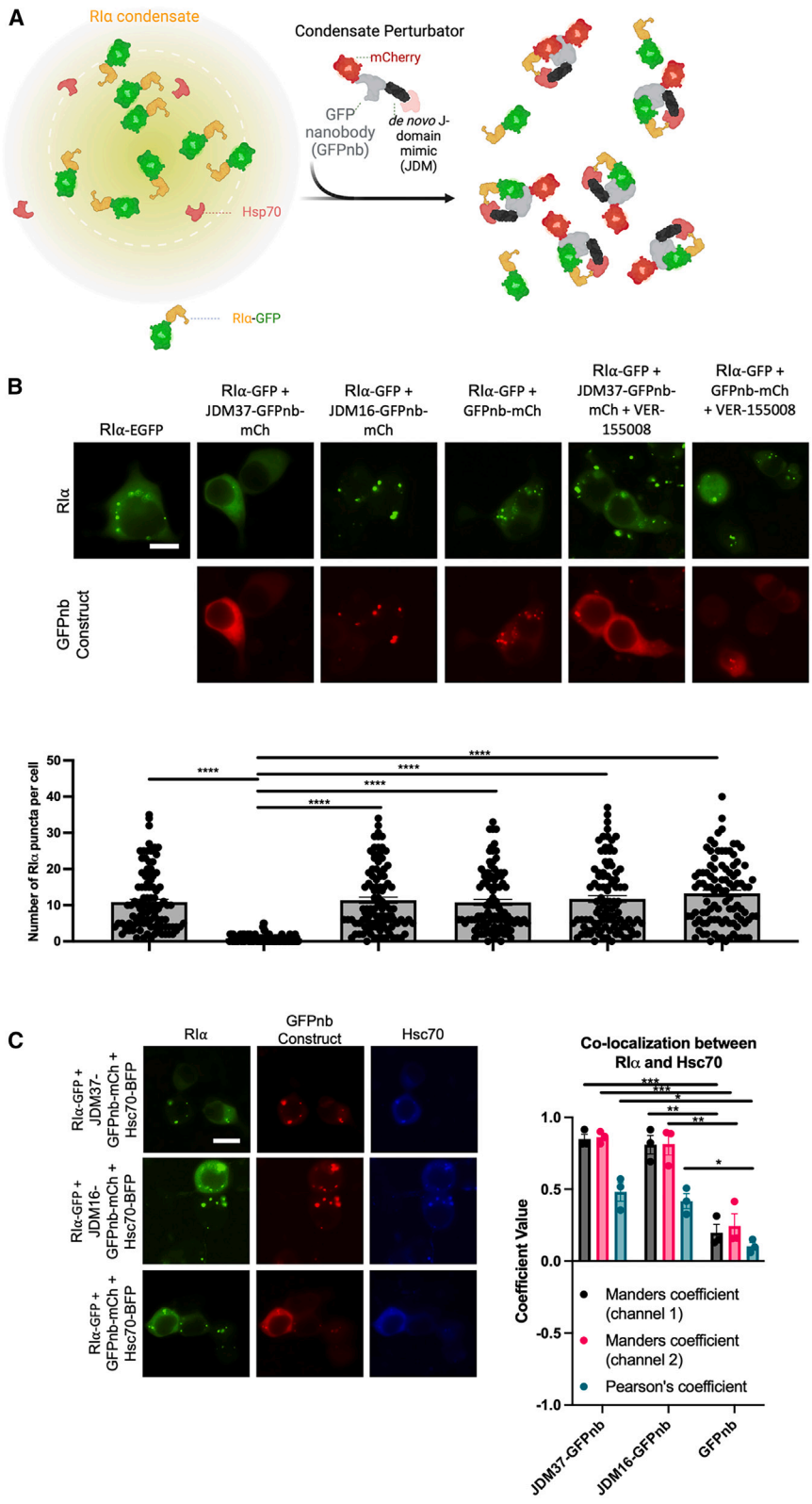

Figure 2. *De novo* Hsp70 activator (JDM37) binds to and activates Hsp70 to dissolve intracellular condensates

(A) Experimental design. The driver of condensation (here, RIα) is fused with GFP. JDM37 is fused to a GFPnb and mCh (JDM37-GFPnb-mCh), and this tool is called condensate perturbator.

(B) Expression of condensate perturbator using JDM37 dissolves GFP-tagged RIα puncta in HEK293T cells. Top: representative epifluorescence images of the various conditions tested in HEK293T cells transfected with the indicated constructs. 1 μM VER-155008 was added for 2 h prior to imaging. Scale bar, 10 μm. Bottom: quantification of number of RIα puncta per cell. Each point represents a single cell (n = 100 cells from 10 independent experiments). Statistics are one-way ANOVA. p values: $^{****}p < 0.0001$.

(C) JDM recruits Hsc70 inside HEK293T cells. Left: representative epifluorescence images of the various conditions tested in HEK293T cells transfected with the indicated constructs. Scale bar, 10 μm. Right: quantitative analysis measuring the co-localization between RIα and Hsc70. Each point represents a separate biological replicate (n = 3 experiments, 51 cells in total for +JDM37-GFPnb, 47 cells in total for +-JDM16-GFPnb, 45 cells in total for +GFPnb). Statistics are two-way Student's t test. p values: $^{*}p < 0.05$, $^{**}p < 0.01$, $^{***}p < 0.001$. See also Figure S7.

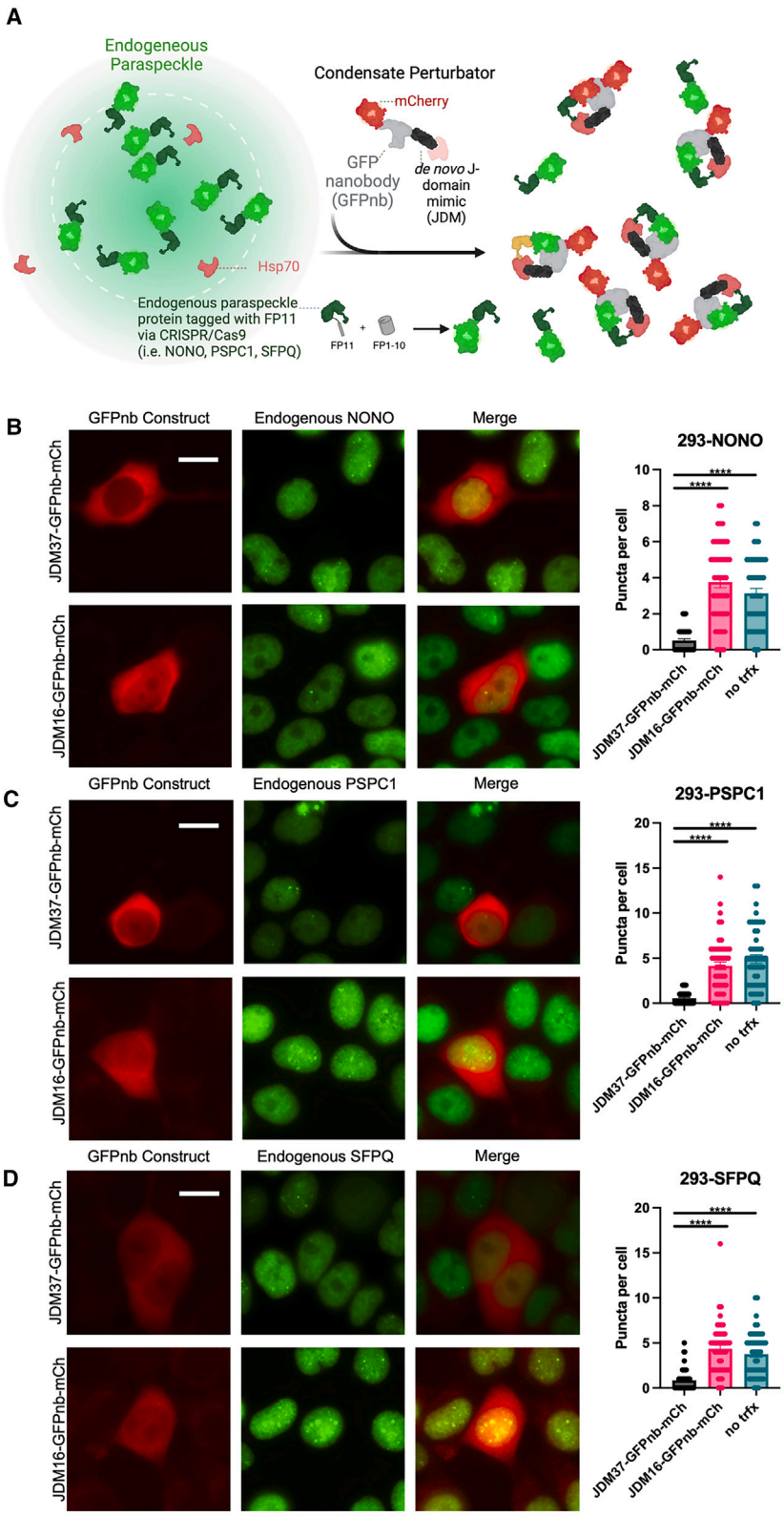

Figure 3. JDM37-mediated dissolution of endogenous condensates

(A) Experimental design. HEK293T cells with the 11th β-strand of mNeonGreen inserted either at the 5′ or 3′ end of an endogenous gene locus and stably co-expressing remaining β-strands of mNeonGreen, thus allowing visualization of proteins expressed at their endogenous level. The proteins studied in this figure are proteins driving paraspeckle formation: NONO, PSPC1, SFPQ. The condensate perturbator here is JDM37-GFPnb-mCh.

(B–D) Expression of JDM37-GFPnb-mCh dissolves GFP-tagged RIα puncta in HEK293T cells that enable visualization of endogenous NONO (293-NONO, B), PSPC1 (293-PSPC1, C), or SFPQ (293-SFPQ, D). Left: representative epifluorescence images of the various conditions tested. Scale bar, 10 μm. Right: quantification of number of paraspeckles per cell. Each point represents a single cell (n = 50 cells). Statistics are one-way ANOVA. p values: ****$p < 0.0001$. See also Figure S8.

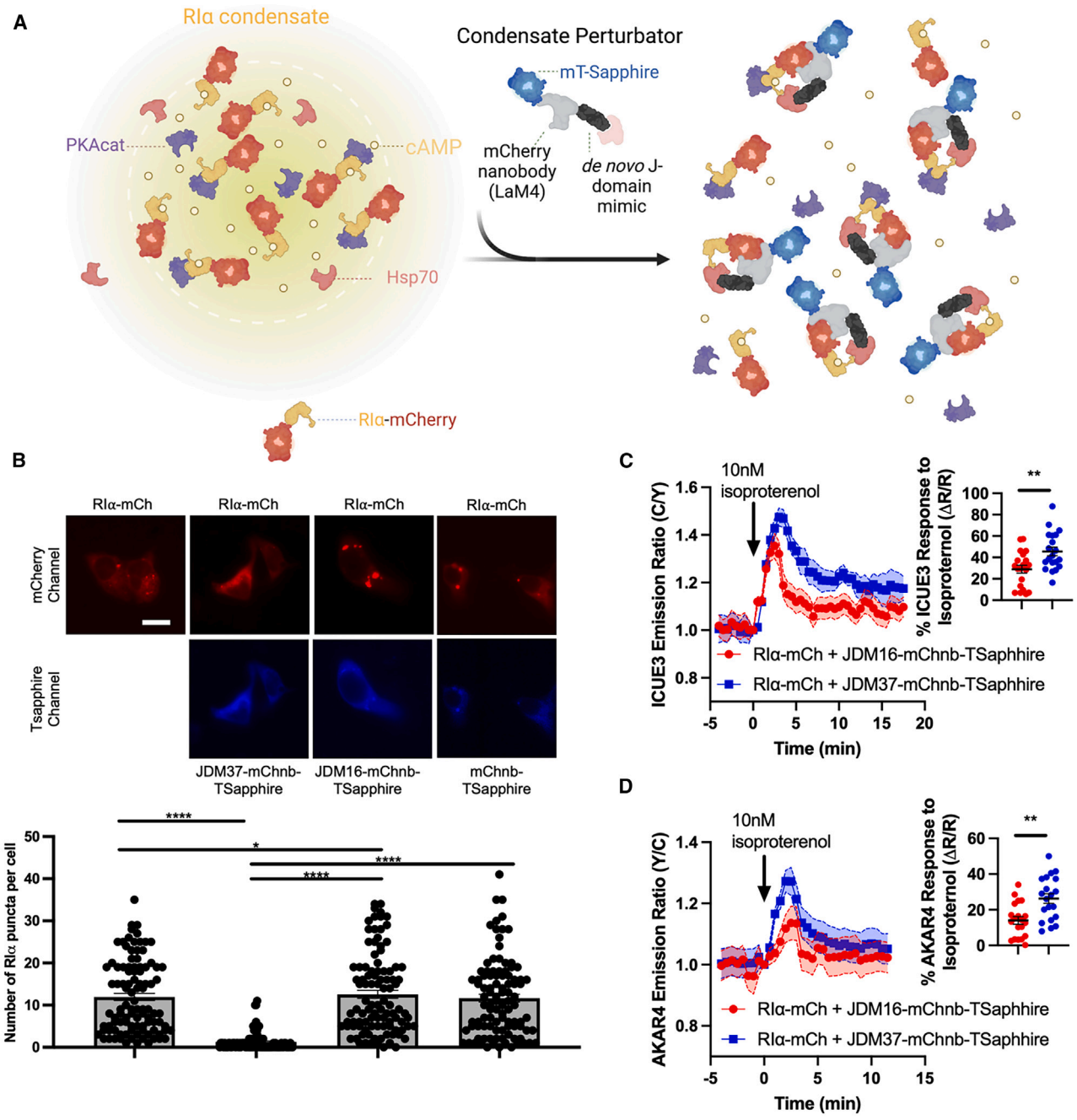

Figure 4. Dissolution of RIα condensates by *de novo* Hsp70 activator (JDM37) leads to global cAMP/PKA signaling increases

(A) Experimental design. The driver of condensation (here, RIα) is fused with mCherry. JDM37 is fused to an mCherry nanobody (mChnb) and mT-Sapphire (TSapphire), and this tool is called condensate perturbator.

(B) Expression of engineered condensate perturbators dissolves mCherry-tagged RIα puncta in HEK293T cells (see STAR Methods for details). Top: representative epifluorescence images of the various conditions tested. Scale bar, 10 μm. Bottom: quantification of number of RIα puncta per cell. Each point represents a single cell (n = 100 cells from 10 independent experiments). For the quantification of number of puncta per cell, cells only with sufficient expression of the condensate perturbator were chosen for analysis (see STAR Methods for details). Statistics are one-way ANOVA. p values: *p < 0.05, ****p < 0.0001.

(C and D) Time-course imaging of HEK293T cells expressing mCherry-tagged RIα, either cAMP sensor ICUE3 (C) or PKA sensor AKAR4 (D), and either JDM37-based or JDM16-based condensate perturbators. In each condition, 10 nM isoproterenol was added (n = at least 15 cells per curve). Statistics are two-way Student's t test. p values: **p < 0.01. See also Figure S9.

JDM37-mChnb-TSapphire in the HEK293T cells decreased ~4-fold the number of RIα-mCh puncta per cell without significantly affecting RIα protein levels (Figures 4B and S9A–S9D). Moreover, RIα-mCh expression did not significantly differ across conditions and did not correlate with the size of RIα puncta in cells, suggesting that our results are not due to bias in overexpressing condensate-driving proteins (Figures S9A and S9E). Either fusing JDM16 to mChnb and TSapphire (JDM16-mChnb-TSapphire) or fusing only mChnb with TSapphire (mChnb-TSapphire) did not decrease the number of RIα-mCh puncta per cell (Figure 4B). In fact, RIα-mCh-expressing cells co-expressing JDM16-mChnb-TSapphire showed increased RIα puncta numbers compared to no co-expression (Figure 4B) possibly due to JDM16 inhibiting Hsc70 activity (Figure 1D) thus enhancing disordered protein regions and enhancing RIα condensate formation; however, this result was not consistently seen when using these tools in other condensate systems. Thus, both Hsp70 recruitment and ATP turnover are required for RIα condensate dissolution in this condensate perturbator system. Dissolving RIα condensates by expression of JDM37-mChnb-TSapphire increased global cAMP accumulation and PKA activation after physiological isoproterenol stimulation, as evidenced by time-course biosensor imaging of untargeted (mostly cytosol localization) ICUE3 and AKAR4 (Figures 4C, 4D, S9F, and S9G), respectively. Global Hsp70 inhibition by VER-155008 did not affect RIα condensate numbers, cAMP levels, nor PKA signaling (Figures S9H and S9I), suggesting that recruitment of Hsp70 by JDM37 to the condensate is required for condensate perturbation. This recruitment could increase the probability of RIα to be a substrate for Hsp70, thus regulating RIα condensation. Expression of JDM37-mChnb-TSapphire prevented the formation of new RIα-mCh condensates after Forskolin + 3-Isobutyl-1-methylxanthine treatment (Figure S9J)..

The fusion oncoprotein EML4-Alk (associated with lung adenocarcinoma) can also form condensates that regulate signaling.[21] However, it is not clear whether the formation of this condensate is strictly necessary for oncogenesis. We targeted the JDM37-mChnb-TSapphire protein to mCh-tagged EML4-Alk (Figure 5A) in Beas2B lung cells and observed a drastic decrease in the number of mCh-EML4-Alk puncta per cell, (Figures 5B and S10A–S10C). As with the RIα condensates, the controls (JDM16-mChnb-TSapphire and mChnb-TSapphire) had no effect and EML4-Alk levels did not drastically differ between conditions (Figure S10D). One of the mechanisms by which EML-Alk condensates are thought to act is by locally activating Ras[21] thus turning on downstream oncogenic signaling nodes such as Erk. Consistent with this idea, dissolution of EML4-Alk puncta by JDM37-mChnb-TSapphire, but not JDM16-mChnb-TSapphire, in Beas2B cells decreased global Ras and Erk signaling, as measured by an untargeted (mostly cytosol localization) Ras-LOCKR-S biosensor[22] and phospho-Erk immunoblotting (Figures 2G and S10D). Expression of JDM37-mChnb-TSapphire in EML4-Alk-expressing Beas2B cells also diminished cell growth by ~4-fold compared to controls (Figures 2H and S10E). Global Hsp70 inhibition by VER-155008 did not affect EML4-Alk condensate numbers, Ras signaling, or cell growth (Figures S10E–S10G), suggesting that local activation of Hsp70 by JDM37 is required for condensate perturbation. These results suggest that the formation of EML4-Alk condensates is critical for oncogenic signaling and cell growth, further highlighting the suitability of this condensate as a putative drug target.

DISCUSSION

The Hsp70-JDP system is an ancient mediator of PQC.[1] To better understand the function of this important complex and enable targeting of Hsp70 chaperone activity to specific cellular regions, we have designed artificial JDPs. The relationship between the structural (Figure S6) and functional (Figure S3) properties of the designs should help guide models of Hsp70 regulation by JDMs; that JDM37 and JDM16 differ at only two positions, but only JDM37 stimulates ATPase activity (Figures 1D and S6H) is particularly notable.

Chimeras of JDM37, but not JDM16, dissolved both RIα and EML4-Alk condensates. We hypothesize that involvement of the chaperone network aids in liquefying these condensates by reducing multivalent interactions contributed by disordered protein regions. We anticipate that this property should extend to other condensate systems that are driven by disordered protein domains, and our *de novo* Hsp70 activator should be a generally useful tool to understand the structure-function relationship of these compartments. The utility and generality of Hsp70-mediated perturbation of other condensate systems will be explored in subsequent studies. More generally, the ability to target Hsp70 to specific subcellular locations and targets with substrate-specific synthetic JDPs should be broadly useful.

Limitations of the study

We were unable to determine the exact mechanism by which JDM37 activates Hsc70. It is striking that two point mutations change an inhibitor into an activator. Binding is not sufficient for Hsc70 activation and JDM37 was not the tightest binder among the JDMs (Figures 1D and S3), thus binding affinity alone is not the determinant for Hsc70 activation. Further diversifying the sequences and topologies of Hsp70 binders should help uncover the molecular determinants of Hsp70 activation. (Figures S1D and S1E).

Although it seems very likely, we were unable to confirm that Hsp70 recruitment and ATPase activity[19] are involved in the regulation of condensates we observe (Figure 2) because complete Hsp70 knockdown is cytotoxic. Future studies will more precisely delineate the biochemical and biophysical mechanisms underlying our observed condensate dissolution phenomena.

RESOURCES AVAILABILITY

Lead contact

Further information and requests for resources and reagents should be directed to and will be fulfilled by the lead contact, Jason Z. Zhang (jzz0428@uw.edu).

Materials availability

All unique/stable reagents generated in this study are available from the lead contact with a completed materials transfer agreement.

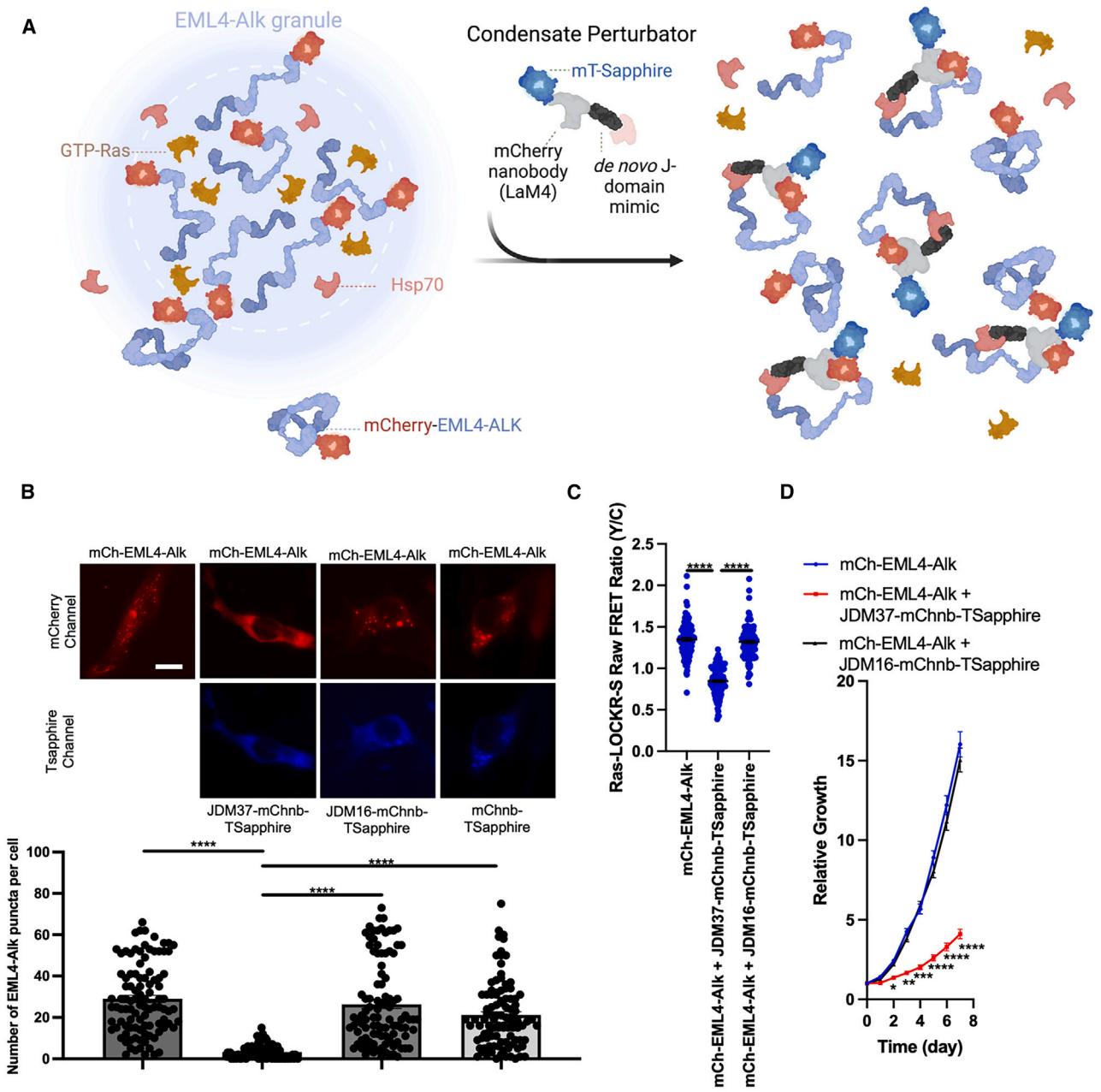

Figure 5. Dissolution of EML4-Alk condensates by JDM37 leads to decreased oncogenic signaling and cell growth

(A) Schematic of strategy to dissolve EML4-Alk oncogenic condensates. Protein that drives condensation (here, EML4-Alk) is tethered with mCherry.

(B) Expression of engineered condensate perturbators dissolves mCherry-tagged EML4-Alk puncta in Beas2B cells (see STAR Methods for details). Top: representative epifluorescence images of the various conditions tested. Scale bar, 10 μm. Bottom: quantification of number of EML4-Alk puncta per cell. Each point represents a single cell (n = 100 cells from 27 independent experiments). For the quantification of number of puncta per cell, cells only with sufficient expression of the condensate perturbator were chosen for analysis (see STAR Methods for details). Statistics are one-way ANOVA. p values: ****$p < 0.0001$.

(C) Raw FRET ratios of Beas2B cells expressing mCherry-tagged EML4-Alk, Ras sensor Ras-LOCKR-S, and either JDM37-based or JDM16-based condensate perturbators. Each point represents a single cell (n = 100 cells from 31 independent experiments). Statistics are two-way Student's t test. p values: ****$p < 0.0001$.

(D) Cell growth curves of Beas2B cells expressing mCherry-tagged EML4-Alk with or without condensate perturbators (n = 3 experiments). Line represents average from all 3 experiments. Statistics are two-way ANOVA. p values: *$p < 0.05$, **$p < 0.01$, ***$p < 0.001$, ****$p < 0.0001$. See also Figure S10.

Data and code availability

- The data that support the findings of this study are on Figshare (https://doi.org/10.6084/m9.figshare.27988496) and are publicly available as of the date of publication. DOIs are listed in the key resources table.
- Code used in this paper is provided in previous work and are listed in the key resources table.
- Any additional information required to reanalyze the data reported in this paper is available from the lead contact upon request.

ACKNOWLEDGMENTS

We acknowledge funding from HHMI (J.Z.Z. and D.B.), Helen Hay Whitney Foundation (J.Z.Z.), the Audacious Project at the Institute for Protein Design (J.Z.Z. and D.B.) and the NIH (NS059690 to J.E.G.). We thank X. Wang, A. Motmaen, and N. Bennett for their help in computational design, S.K. Williams for providing biotinylated Hsc70, S. Vaid for the endogenously tagged cell lines, C. Dobbins for help in mammalian cell culture, I.C. Haydon for providing some schematics in the manuscript, and M.M. Schneider for providing useful feedback on the project.

AUTHOR CONTRIBUTIONS

J.Z.Z. conceived of the project. J.Z.Z., J.E.G., and D.B. supervised, designed, and interpreted the experiments. J.Z.Z. designed the binders with the help from B.H. for the partially *de novo* JDMs. J.Z.Z. and N.G. purified and tested the binders. J.H. tested binders in the *in vitro* activity assays. J.Z.Z. performed the mammalian cell experiments. J.T.C. and C.Q. designed and performed the *E. coli* growth experiments. B.D.R. helped with discussion for the sequence and structure comparisons. J.Z.Z., J.E.G., and D.B. wrote the original draft. All authors reviewed and commented on the manuscript.

DECLARATION OF INTERESTS

The authors declare no competing interests.

STAR★METHODS

Detailed methods are provided in the online version of this paper and include the following:

- KEY RESOURCES TABLE
- EXPERIMENTAL MODEL AND STUDY PARTICIPANT DETAILS
  - Cell culture and transfection
- METHOD DETAILS
  - Designing partially *de novo* J-domain mimics
  - Designing fully *de novo* J-domain mimics
  - DNA library preparation
  - Yeast surface display
  - Biolayer interferometry
  - Bacterial protein production and purification
  - Hsc70 ATP turnover assay
  - Luciferase refolding assay
  - Bacterial cell growth assays
  - Immunoblotting and immunoprecipitation
  - Cell counting to measure cell proliferation
  - Epifluorescence imaging
- QUANTIFICATION AND STATISTICAL ANALYSIS
  - FRET biosensor analysis
  - Quantification of cellular puncta
  - Statistics and reproducibility

SUPPLEMENTAL INFORMATION

Supplemental information can be found online at https://doi.org/10.1016/j.chembiol.2025.01.006.

Received: July 23, 2024
Revised: October 29, 2024
Accepted: January 9, 2025
Published: February 7, 2025

REFERENCES

1. Hyman, A.A., Weber, C.A., and Jülicher, F. (2014). Liquid-Liquid Phase Separation in Biology. Annu. Rev. Cell Dev. Biol. *30*, 39–58.
2. Zhang, J.Z., Lu, T.W., Stolerman, L.M., Tenner, B., Yang, J.R., Zhang, J.F., Falcke, M., Rangamani, P., Taylor, S.S., Mehta, S., and Zhang, J. (2020). Phase separation of a PKA regulatory subunit controls cAMP compartmentation and oncogenic signaling. Cell *182*, 1531–1544.e15.
3. Kampinga, H.H., Andreasson, C., Barducci, A., Cheetham, M.E., Cyr, D., Emanuelsson, C., Genevaux, P., Gestwicki, J.E., Goloubinoff, P., Huerta-Cepas, J., et al. (2019). Function, evolution, and structure of J-domain proteins. Cell Stress Chaperones *24*, 7–15.
4. Kampinga, H.H., and Craig, E.A. (2010). The HSP70 chaperone machinery: J proteins as drivers of functional specificity. Nat. Rev. Mol. Cell Biol. *11*, 579–592.
5. Piette, B.L., Alerasool, N., Lin, Z.Y., Lacoste, J., Lam, M.H.Y., Qian, W.W., Tran, S., Larsen, B., Campos, E., Peng, J., et al. (2021). Comprehensive interactome profiling of the human Hsp70 network highlights functional differentiation of J domains. Mol. Cell *81*, 2549–2565.e8.
6. Yu, H., Lu, S., Gasior, K., Singh, D., Vazquez-Sanchez, S., Tapia, O., Toprani, D., Beccari, M.S., Yates, J.R., 3rd, Da Cruz, S., et al. (2021). HSP70 chaperones RNA-free TDP-43 into anisotropic intranuclear liquid spherical shells. Science *371*, eabb4309.
7. Rosenzweig, R., Nillegoda, N.B., Mayer, M.P., and Bukau, B. (2019). The Hsp70 chaperone network. Nat. Rev. Mol. Cell Biol. *20*, 665–680.
8. Clerico, E.M., Tilitsky, J.M., Meng, W., and Gierasch, L.M. (2015). How Hsp70 Molecular Machines Interact with Their Substrates to Mediate Diverse Physiological Functions. J. Mol. Biol. *427*, 1575–1588.
9. Faust, O., Abayev-Avraham, M., Wentink, A.S., Maurer, M., Nillegoda, N.B., London, N., Bukau, B., and Rosenzweig, R. (2020). HSP40 proteins use class-specific regulation to drive HSP70 functional diversity. Nature *587*, 489–494.
10. Turnham, R.E., Smith, F.D., Kenerson, H.L., Omar, M.H., Golkowski, M., Garcia, I., Bauer, R., Lau, H.T., Sullivan, K.M., Langeberg, L.K., et al. (2019). An acquired scaffolding function of the DNAJ-PKAc fusion contributes to oncogenic signaling in fibrolamellar carcinoma. Elife *8*, e44187.
11. Cao, L., Coventry, B., Goreshnik, I., Huang, B., Sheffler, W., Park, J.S., Jude, K.M., Marković, I., Kadam, R.U., Verschueren, K.H.G., et al. (2022). Design of protein-binding proteins from the target structure alone. Nature *605*, 551–560.
12. An, L., and Lee, G.R. (2020). De Novo Protein Design Using the Blueprint Builder in Rosetta. Curr. Protoc. Protein Sci. *102*, e116.
13. Kityk, R., Kopp, J., and Mayer, M.P. (2018). Molecular mechanism of J-domain-triggered ATP hydrolysis by Hsp70 chaperones. Mol. Cell *69*, 227–237.e4.
14. Tiwari, S., Fauvet, B., Assenza, S., De Los Rios, P., and Goloubinoff, P. (2023). fluorescent multi-domain protein reveals the unfolding mechanism of Hsp70. Nat. Chem. Biol. *19*, 198–205.
15. Imamoglu, R., Balchin, D., Hayer-Hartl, M., and Hartl, F.U. (2020). Bacterial Hsp70 resolves misfolded states and accelerates productive folding of a multi-domain protein. Nat. Commun. *11*, 365.
16. Nillegoda, N.B., Kirstein, J., Szlachcic, A., Berynskyy, M., Stank, A., Stengel, F., Arnsburg, K., Gao, X., Scior, A., Aebersold, R., et al. (2015). Crucial HSP70 co-chaperone complex unlocks metazoan protein disaggregation. Nature *524*, 247–251.
17. Prole, D.L., and Taylor, C.W. (2019). A genetically encoded toolkit of functionalized nanobodies against fluorescent proteins for visualizing and manipulating intracellular signaling. BMC Biol. *17*, 41.
18. Petrucelli, L., Dickson, D., Kehoe, K., Taylor, J., Snyder, H., Grover, A., De Lucia, M., McGowan, E., Lewis, J., Prihar, G., et al. (2004). CHIP and Hsp70 regulate tau ubiquitination, degradation and aggregation. Hum. Mol. Genet. *13*, 703–714.
19. Cho, N.H., Cheveralls, K.C., Brunner, A.D., Kim, K., Michaelis, A.C., Raghavan, P., Kobayashi, H., Savy, L., Li, J.Y., Canaj, H., et al. (2022).

OpenCell: Endogenous tagging for the cartography of human cellular organization. Science *375*, eabi6983.

20. Fox, A.H., Nakagawa, S., Hirose, T., and Bond, C.S. (2018). Paraspeckles: where long noncoding RNA meets phase separation. Trends Biochem. Sci. *43*, 124–135.
21. Tulpule, A., Guan, J., Neel, D.S., Allegakoen, H.R., Lin, Y.P., Brown, D., Chou, Y.T., Heslin, A., Chatterjee, N., Perati, S., et al. (2021). Kinase-mediated RAS signaling via membraneless cytoplasmic protein granules. Cell *184*, 2649–2664.e18.
22. Zhang, J.Z., Nguyen, W.H., Greenwood, N., Rose, J.C., Ong, S.E., Maly, D.J., and Baker, D. (2024). Computationally designed sensors detect endogenous Ras activity and signaling effectors at subcellular resolution. Nat. Biotechnol. *42*, 1888–1898.
23. Leu, J.I.-J., Zhang, P., Murphy, M.E., Marmorstein, R., and George, D.L. (2014). Structural Basis for the Inhibition of HSP70 and DnaK Chaperones by Small-Molecule Targeting of a C-Terminal Allosteric Pocket. ACS Chem. Biol. *9*, 2508–2516.
24. Taylor, I.R., Dunyak, B.M., Komiyama, T., Shao, H., Ran, X., Assimon, V.A., Kalyanaraman, C., Rauch, J.N., Jacobson, M.P., Zuiderweg, E.R.P., and Gestwicki, J.E. (2018). High-throughput screen for inhibitors of protein and protein interactions in a reconstituted heat shock protein 70 (Hsp70) complex. J. Biol. Chem. *293*, 4014–4025.

STAR★METHODS

KEY RESOURCES TABLE

REAGENT or RESOURCE	SOURCE	IDENTIFIER
Antibodies		
Ms anti-Erk	CST	Cat#9107
Rb anti-phospho-Erk	CST	Cat#9101
Ms anti-Vinculin	Sigma-Aldrich	Cat#V9131
Ms anti-Myc Tag	CST	Cat#2276
Ms anti-Flag Tag	Sigma-Aldrich	Cat#A8592
Rb anti-GFP	CST	Cat#2555
Rb anti-Hsp70	CST	Cat#4872
Rb anti-BiP	CST	Cat#3177
Ms anti-Hsp72	Millipore	Cat#MABE1130
Rb anti-NONO	CST	Cat#90336
Rb anti-PSPC1	CST	Cat#65992
Rb anti-SFPQ	CST	Cat#71992
Rb anti-GAPDH	CST	Cat#5174
Streptavidin, Alexa Fluor™ 488 conjugate	ThermoFisher	Cat#S11223
anti-C-Myc Antibody (Chicken) - FITC Conjugated	ICL	Cat#CMYC-45F
680 RD anti-Ms	LICOR	Cat#26-68071
680 RD anti-Rb	LICOR	Cat#926-68070
800 CW anti-Ms	LICOR	Cat#926-32210
800 CW anti-Rb	LICOR	Cat#926-32211
Bacterial and virus strains		
E. coli Lemo21(DE3)	NEB	Cat#C2527
S. cerevisiae EBY100	Phageomics	Cat#YEC001
Chemicals, peptides, and recombinant proteins		
Hsc70	This paper	N/A
NRLLLTG peptide	Genscript	N/A
BugBuster Protein Extraction buffer	Millipore	Cat#70921
DnaJA2	This paper	N/A
Fugene HD Transfection Reagent	Fugene	Cat#E2311
Poly-D-Lysine	MP Biomedical	Cat#215017580
RIPA Buffer	Thermo Fisher	Cat#89901
Lipofectamine™ LTX Reagent with PLUS™ Reagent	Thermo Fisher	Cat#15338100
Turbofectin 8.0	Origene	Cat#TF81001
Electroporation Buffer	MaxCyte	Cat#EPB-5
16% PFA	Electron Microscopy Services	Cat#15710
Trans-Blot Turbo Transfer Pack	BioRad	Cat#1704159
Pierce Protease Inhibitor Tablets	Thermo Fisher	Cat#A32963
PHEM 0.2M	Electron Microscopy Services	Cat#11165
Biotin	Sigma-Aldrich	Cat#B4501
0.25% Trypsin-EDTA	Gibco	Cat#25200072
Pageruler Prestained Ladder	Thermo Fisher	Cat#PI26620
Spectra™ Multicolor High Range Protein Ladder	Thermo Fisher	Cat#26625
Protein A Agarose Beads	CST	Cat#9863S
Protein G Agarose Beads	CST	Cat#37478
Puromycin	Tocris	Cat#4089
Hygromycin	Tocris	Cat#4137

(*Continued on next page*)

Continued

REAGENT or RESOURCE	SOURCE	IDENTIFIER
DPBS	Gibco	Cat#14190250
Doxycycline	Tocris	Cat#4090
Studier Induction Media	Teknova	Cat#3S8000
Kanamycin	Millipore Sigma	Cat#PHR1487
Ni-NTA resin	Qiagen	Cat#30250
Ultra-15 Centrifugal Filter Units	Amicon	Cat#UFC9100
Superdex 75 Increase 10/300 GL	GE Healthcare	Cat#29148721
EGF	Thermo Fisher	Cat#PHG0311
Polydiallyldimethylammonium	Sigma-Aldrich	Cat#409014
Talon cobalt affinity resin	Takara Bio	Cat#635653
Cytiva S200 Increase column	Sigma-Aldrich	Cat#GE28-9909-44
DAPI	ThermoFisher	Cat#62248
FluoroBrite DMEM Media	GIBCO	Cat#A1896701
FBS	Sigma-Aldrich	Cat#F2442
Pen-Strep	Sigma-Aldrich	Cat#P4333
RPMI 1640	GIBCO	Cat#11875093
PEI Max	PolyScience	Cat#24765
Steady Glo	Promega	Cat#E2510
Creatine kinase	This paper	N/A
NEF	This paper	N/A
Firefly luciferase	Promega	Cat#G7940
Critical commercial assays		
BirA bulk kit	Avidity LLC	Cat#EC 6.3.4.15
Kapa HiFi Polymerase	Roche	Cat#07958927001
QIAquick gel extraction kits	Qiagen	Cat#28706
QIAquick Clean up kit	Qiagen	Cat#28506
Zymoprep yeast extraction kit	Zymo Research	Cat#D2004
Deposited data		
Combined data	Figshare	figshare.com/articles/dataset/dx_doi_org_10_6084_m9_figshare_6025748/6025748 https://doi.org/10.6084/m9.figshare.27988496
Experimental models: Cell lines		
HEK293T	ATCC	Cat#CRL-3216
Beas2B	ATCC	Cat#CRL-9609
HEK293T endogenously tagged cell lines	Chan Zuckerberg Biohub, OpenCell Initative	N/A
Recombinant DNA		
ICUE3	Zhang et al.[2]	N/A
AKAR4	Zhang et al.[2]	N/A
Ras-LOCKR-S	Zhang et al.[22]	N/A
PETCON3 JDM designs	This paper	N/A
pET29b+ JDM designs	This paper	N/A
pET29b+ DnaJ	This paper	N/A
pcDNA3 JDM-GFPnb-mCh	This paper	N/A
pcDNA3 JDM-mChnb-TSapphire	This paper	N/A
pcDNA3 Hsc70	This paper	N/A
Software and algorithms		
Rosetta	RosettaCommons	docs.rosettacommons.org/demos/latest/tutorials/install_build
AlphaFold2	DeepMind	Github.com/google-deepmind/alphafold

(*Continued on next page*)

Continued		
REAGENT or RESOURCE	SOURCE	IDENTIFIER
Blueprint Builder	An, L. and Lee, G. R.[12]	Github.com/LAnAlchemist/blueprint_builder_demo
RIFdock	Cao L. et al.[11]	Github.com/rifdock/rifdock
ForteBio Data Analysis	ForteBio	v.9.0.0.14
ImageJ	NIH LOCI	v2.14.0/1.54f
GraphPad Prism	GraphPad	v10.4.0
Other		
Streptavidin Octet tips	Sartorius	Cat#18-5021
LightCycler480 Sealing Foil	Roche	Cat#04729757001

EXPERIMENTAL MODEL AND STUDY PARTICIPANT DETAILS

Cell culture and transfection

HEK293T and endogenously tagged HEK293T cells were cultured in Dulbecco's modified Eagle medium (DMEM) containing 1 g L^{-1} glucose and supplemented with 10% (v/v) fetal bovine serum (FBS) and 1% (v/v) penicillin–streptomycin (Pen-Strep). Beas2B cells were cultured in Roswell Park Memorial Institute 1640 (RPMI 1640) with 10% (v/v) FBS and 1% Pen-Strep. All cells were grown in a humidified incubator at 5% CO_2 and at 37°C.

Before transfection, all cells were plated onto sterile poly-D-lysine coated plates or dishes and grown to 50%–70% confluence. HEK293T and Beas2B cells were transfected using Turbofectin 8 and grown for an either an additional 16-24 hours for HEK293T or 48 hours for Beas2B before imaging. Beas2B cells underwent serum starvation for 16-24 hours prior to downstream experiments.

Sex of cell lines used here have been characterized previously by suppliers: HEK293T (female), Beas2B (male). Cell lines were authenticated by suppliers but not in our hands.

METHOD DETAILS

Designing partially *de novo* J-domain mimics

The crystal structure (PDB: 5NRO) of the J-domain-activated conformation of DnaK (ATP-loaded DnaK bound to the J-domain of DnaJ) was refined with the Rosetta FastRelax protocol with coordinate constraints. Miniprotein binder generation began by paring down J-domain by removing its first and fourth helix as they do not directly interact with DnaK. Afterwards, a third helix on top of the remaining helices were added by using the RosettaRemodel blueprint[12] program in order to increase stability of the remaining helices. 30,000 blueprints that differed in the lengths of the helices and the loop types were generated. The whole miniprotein except the key interacting residues on the J-domain were then designed using the FastDesign protocol. From these designs, the monomeric metrics and the interface metrics were calculated using Rosetta and these metrics were used to filter designs based on maintaining the shape of the interacting helices (particularly the HPD motif geometry). Top 15,000 designs were selected for AlphaFold2 structure predictions in complex with DnaK and these predicted complexes were again calculated for interface metrics using Rosetta. These metrics were used to identify the top 5,000 designs based on its predicted binding to DnaK. This protocol is graphically summarized in Figure S1D.

Designing fully *de novo* J-domain mimics

This protocol has been described previously.[11] In brief, the crystal structure (PDB: 5NRO) of the J-domain-activated conformation of DnaK (ATP-loaded DnaK bound to the J-domain of DnaJ) was refined with the Rosetta FastRelax protocol with coordinate constraints, and the J-domain was extracted for subsequent steps. Initial docking conformations were generated by RifDock. Next, billions of individual disembodied amino acids were docked against DnaK using RifDock and specifying the dock with residues (6-10) on DnaK that interact with DnaJ based on 5NRO. The ones that passed a specific energy cutoff value (-1.5 Rosetta energy unit) were stored and the corresponding inverse rotamers were generated. The *de novo* scaffold library of 19,000 miniproteins (in length 56 - 65 residues, mostly three helical bundles) were docked into the field of the inverse rotamers to produce initial docked conformations. These docked conformations were further optimized using the FastDesign protocol to generate shape and chemically complementary interfaces. Computational metrics of the final design models were calculated using Rosetta, which includes ddg, shape complementary, contact patch, and interface buried solvent accessible surface area. The designs that scored well in these interface metrics were analyzed for common motifs (couple amino acids in length) and these privileged motifs were fed into MotifGraft to build the next set of miniproteins. Afterwards, these next set of designs were again ran through FastDesign. 2,000,000 of these designs were then predicted in AlphaFold2 structure predictions in complex with DnaK and these predicted complexes were again calculated for interface metrics using Rosetta. Several iterations of FastDesign, MotifGraft, and AlphaFold2 were performed, as diagrammed in Figure S1D. After final AlphaFold2 predictions and metric scoring, the top 25,000 designs based on its predicted binding to DnaK were ordered.

DNA library preparation

All protein sequences were padded to a uniform length (65 amino acids) by adding a (GGGS)n linker at the C terminal of the designs, to avoid the biased amplification of short DNA fragments during PCR reactions. The protein sequences were reversed translated and optimized using DNAworks2.0 with the S. cerevisiae codon frequency table. Homologous to the pETCON plasmid Oligo libraries encoding the designs were ordered from Twist Bioscience. Oligo pool encoding the *de novo* designs and the point mutant library for SSM were ordered from Agilent Technologies. Combinatorial libraries were ordered as Integrated DNA Technologies ultramers with the final DNA diversity ranging from 1×10^6 to 1×10^7.

All libraries were amplified using Kapa HiFi Polymerase with a BioRAD CFX96 qPCR machine. In detail, the libraries were firstly amplified in a 25 μL reaction, and PCR reaction was terminated when the reaction reached half the maximum yield to avoid over-amplification. The PCR product was loaded to a DNA agarose gel. The band with the expected size was cut out and DNA fragments were extracted using QIAquick kits. Then, the DNA product was re-amplified as before to generate enough DNA for yeast transformation. The final PCR product was cleaned up with a QIAquick Clean up kit. For the yeast transformation, 2-3 μg of digested modified pETcon vector (pETcon3) and 6 μg of insert were transformed into EBY100 yeast strain using the protocol as described before.

DNA libraries for deep sequencing were prepared using the same PCR protocol, except the first step started from yeast plasmid prepared from 5×10^7 to 1×10^8 cells by Zymoprep. Illumina adapters and 6-bp pool-specific barcodes were added in the second qPCR step. Gel extraction was used to get the final DNA product for sequencing. All libraries include the native library and different sorting pools were sequenced using Illumina NextSeq/MiSeq sequencing.

All pcDNA3.1 plasmids constructed here were produced by GenScript.

Yeast surface display

S. cerevisiae EBY100 strain cultures were grown in C-Trp-Ura media and induced in SGCAA media following the protocol as described before. Cells were washed with PBSF (PBS with 1% BSA) and labelled with biotinylated Hsc70 using two labeling methods, with-avidity and without-avidity labeling. For the with-avidity method, the cells were incubated with biotinylated Hsc70, together with anti-c-Myc fluorescein isothiocyanate (FITC) and streptavidin–phycoerythrin (SAPE). The concentration of SAPE in the with-avidity method was used at 1/4 concentration of the biotinylated Hsc70. The with-avidity method was used in the first few rounds of screening of the original design to fish out weak binder candidates. For the without-avidity method, the cells were firstly incubated with biotinylated Hsc70, washed, secondarily labeled with SAPE and FITC. For these designs, three rounds of with-avidity sorts were applied at 1 μM concentration of Hsc70 (HSPA8), 5 mM ATP, 1 μM NR peptide (NRLLLTG,[23] with N-terminal acetylation) to occupy Hsc70's substrate binding domain, 5 mM $MgCl_2$, and 10 mM KCl. For the original library of *de novo* designs, the library was sorted twice using the with-avidity method at 1 μM Hsc70, followed by several without-avidity sorts in the third round of sorting with Hsc70 concentrations at 1 μM, 100 nM and 10 nM. The SSM library was screened using the without-avidity method for four rounds, with Hsc70 concentrations at 1 μM, 100 nM, 10 nM and 1 nM. The combinatorial libraries were sorted to convergence by decreasing the target concentration with each subsequent sort and collecting only the top 0.1% of the binding population. The final sorting pools of the combinatorial libraries were sequenced using Illumina NextSeq/MiSeq sequencing.

Biolayer interferometry

Biolayer interferometry binding data were collected in an Octet RED96 and processed using the instrument's integrated software. For minibinder binding assays, biotinylated Hsc70 was loaded onto streptavidin-coated biosensors at 50 nM in binding buffer (10 mM HEPES (pH 7.4), 150 mM NaCl, 3 mM EDTA, 0.05% surfactant P20, 0.5% non-fat dry milk) along with 5 mM ATP, 1 μM NR peptide, 5mM $MgCl_2$, and 10 mM KCl for 360 s. Analyte proteins were diluted from concentrated stocks into binding buffer. After baseline measurement in the binding buffer alone, the binding kinetics were monitored by dipping the biosensors in wells containing the target protein at the indicated concentration (association step) and then dipping the sensors back into baseline/buffer (dissociation). Data were analyzed and processed using ForteBio Data Analysis software v.9.0.0.14.

Bacterial protein production and purification

For all the JDMs, DnaJB1, DnaJA2 J-domain only ($DnaJA2^{1-68}$), and Hsc70 (HSPA8), the *E. coli* Lemo21(DE3) strain was transformed with a $pET29b^+$ plasmid encoding the synthesized gene of interest. Cells were grown for 24 hour in liquid broth medium supplemented with kanamycin. Cells were inoculated at a 1:50 mL ratio in the Studier TBM-5052 autoinduction medium supplemented with kanamycin, grown at 37°C for 2–4 hours and then grown at 18°C for an additional 18 hours. Cells were collected by centrifugation at 4,000 *g* at 4°C for 15 min and resuspended in 30 mL lysis buffer (20 mM Tris-HCl, pH 8.0, 300 mM NaCl, 30 mM imidazole, 1 mM PMSF and 0.02 mg ml^{-1} DNase). Cell resuspensions were lysed by sonication for 2.5 min (5 s cycles). Lysates were clarified by centrifugation at 24,000 xg at 4°C for 20 min and passed through Ni-NTA nickel resin (2 mL) pre-equilibrated with wash buffer (20 mM Tris-HCl, pH 8.0, 300 mM NaCl and 30 mM imidazole). The resin was washed twice with 10 column volumes of wash buffer, and then eluted with elution buffer (20 mM Tris-HCl, pH 8.0, 300 mM NaCl and 300 mM imidazole). The eluted proteins were concentrated using Ultra-15 Centrifugal Filter Units and further purified by using either Superdex 75 Increase 10/300 GL or Superdex 200 Increase 10/300 GL (depending on kDa of protein) size exclusion column in TBS (25 mM Tris-HCl, pH 8.0, and 150 mM NaCl). Fractions containing monomeric protein were pooled, concentrated and snap-frozen in liquid nitrogen and stored at −80°C.

Biotinylation of purified Hsc70 was performed using the BirA bulk kit according to manufacturer's protocol. Briefly, biotinylation reactions (pH 8.0; 1:1 ratio) were performed overnight at 4°C on an orbital shaker and then excess biotinylation reagent was removed

using Superdex 200 Increase 10/300 GL (depending on kDa of protein) size exclusion column in TBS (25 mM Tris-HCl, pH 8.0, and 150 mM NaCl).

To purify the JDMs fused to DnaJ (DnaJ Δ^{1-70}), the same protocol as above was performed, except the cells were inoculated in Terrific Broth II buffer supplemented with kanamycin, grown at 37°C until OD_{600} 0.5 to 1, IPTG (0.2 mM) was added, and then the bacteria were grown at 37°C overnight. Cells were also lysed in BugBuster Protein Extraction buffer for 30 min instead of sonication.

Hsc70 ATP turnover assay

Hsc70's ATPase activity was measured via a quinaldine red-based fluorescence assay as described before.[24] In brief, a dilution series of either DnaJA2 or JDMs was prepared and added to Hsc70 (1 μM) in 384-well plates using a Multidrop dispenser. Quinaldine red solution was freshly prepared each day as a 2:1:1:2 ratio of 0.05% w/v quinaldine red, 2% w/v polyvinyl alcohol, 6% w/v ammonium molybdate tetrahydrate in 6 M HCl. To each well of a 384-well white, low-volume, polystyrene plate was added 5 μL of the chaperone mixture. The assay buffer (100 mM Tris, 20 mM KCl, 6 mM $MgCl_2$, pH 7.4), was supplemented with 0.01% Triton X-100 to avoid identifying aggregation. Then, 5 μL of 5 mM ATP was added to initiate the reaction. The plates were centrifuged briefly, and subsequently incubated at 37 °C for 1 to 2 hrs. After incubation, 15 μL of quinaldine red solution was added, and after a 15 minute incubation, 2 μL sodium citrate (32% w/v) was added to quench the reaction. After another 15-min incubation period at 37°C, fluorescence (excitation 430 nm, emission 530 nm) was measured in a PHERAstar plate reader.

Luciferase refolding assay

Luciferase refolding assays followed a previously described procedure.[24] In brief, native firefly luciferase was denatured in 8 M guanidine hydrochloride for at least 1 hour at room temperature and then diluted into assay buffer (28 mM HEPES, pH 7.6, 120 mM potassium acetate, 12 mM magnesium acetate, 2.2 mM dithiothreitol, 8.8 mM creatine phosphate, and 35 units/ml creatine kinase). Solutions were prepared of test samples (e.g., DnaJA2, JDMs), 1 μM Hsc70, 0.125μM NEF, denatured luciferase (at 0.1 μM), and 1 mM ATP. Total volume was 25 μL in white 96-well plates, and incubation time was 1 hour at 37°C. Steady Glo reagent was prepared fresh and added to the plate immediately prior to reading luminescence.

Bacterial cell growth assays

Single colonies from freshly transformed cells were used to inoculate 5 mL cultures of LB media containing the antibiotics required to maintain plasmids. For testing effects of JDM on WT *E. coli*, the *E. coli* Lemo21(DE3) strain was transformed with a $pET29b^+$ plasmid encoding the synthesized gene of interest and cells were then grown for 24 hour in liquid broth medium supplemented with kanamycin. For growth assays, 4 μL of resuspended cells (~1 × 106 cells) were used to inoculate each well of a 96-well plate containing 196 μL of LB media (supplemented with ampicillin, and 200uM IPTG). The plate was covered with transparent LightCycler480 Sealing Foil, and grown for 24 h in a Biotek Synergy H1 plate reader at 42°C with double orbital shaking, measuring OD_{600} every 10 min. Max-V was determined by measuring maximal growth over 15 measurements.

Immunoblotting and immunoprecipitation

Cells expressing indicated constructs and incubated with indicated drugs were plated, transfected, and labeled as described in figure legends. Cells were then transferred to ice and washed 2x with ice cold DPBS. Cells were then detached from the well by addition of 1x RIPA lysis buffer (50 mM Tris pH 8, 150 mM NaCl, 0.1% SDS, 0.5% sodium deoxycholate, 1% Triton X-100, 1x protease inhibitor cocktail, 1 mM PMSF, 1mM Na_3VO_4, 1% NP-40) and either scraping of cells or rotation on shaker for 30 min at 4°C. Cells were then collected and vortexed for at least 5 s every 10 min for 20 min at 4°C. Cells were then collected and clarified by centrifugation at 20,000 rpm for 10 minutes at 4°C. The supernatant was collected and underwent Pierce BCA assay to quantify total protein amounts.

For immunoblotting, whole cell lysate protein amounts were normalized across samples in the same gel, mixed with 4x loading buffer prior to loading, incubated at 95°C for 5 min and then 4°C for 5 min, and separated on Any kDa SDS-PAGE gels. Proteins separated on SDS-page gels were transferred to nitrocellulose membranes via the TransBlot system. The blots were then blocked in 5% milk (w/v) in TBST (Tris-buffered saline, 0.1% Tween 20) for 1 hour at room temperature. Blots were washed with TBST 3x then incubated with indicated primary antibodies in 1% BSA (w/v) in TBST overnight at 4°C. Blots were then washed with TBST 3x and incubated with LICOR dye-conjugated secondary antibodies (LICOR 680/800 or streptavidin-LICOR 800) in 1% BSA (w/v) in TBST for 1 hour at room temperature. The blots were washed with TBST 3x and imaged on an Odyssey IR imager. Quantitation of Western blots was performed using ImageJ on raw images.

For immunoprecipitation, agarose beads were washed 3x lysis buffer washes and then antibodies were loaded by adding 1mg ml^{-1} indicated antibodies at 4°C on orbital shaker for 3 hour. Beads were then washed 2x in lysis buffer. Whole cell lysate protein amounts were normalized across samples and protein samples were added to beads (at least 100 μ g per sample) at 4°C on orbital shaker overnight. Beads were then washed 2x in lysis buffer and 1x in TBS and then mixed with 4x loading buffer. The remaining portion of the protocol is the same as immunoblotting.

Cell counting to measure cell proliferation

Beas2B cell lines were seeded in 6-wells plates at 10,000 cells/well. Cell numbers were quantified using a hemacytometer each day for 7 days.

Epifluorescence imaging

Cells were washed twice with FluoroBrite DMEM imaging media and subsequently imaged in the same media in the dark at room temperature. Isoproterenol was added as indicated. Epifluorescence imaging was performed on a Yokogawa CSU-X1 spinning dish confocal microscope with either a Lumencor Celesta light engine with 7 laser lines (408, 445, 473, 518, 545, 635, 750 nm) or a Nikon LUN-F XL laser launch with 4 solid state lasers (405, 488, 561, 640 nm), 40x/0.95 NA objective and a Hamamatsu ORCA-Fusion scientific CMOS camera, both controlled by NIS Elements 5.30 software (Nikon). The following excitation/FRET filter combinations (center/bandwidth in nm) were used: CFP: EX445 EM483/32, CFP/YFP FRET: EX445 EM542/27, YFP: EX473 EM544/24, GFP: EX473 EM525/36, RFP (mCherry): EX545 EM605/52, TSapphire: EX405 EM525/36. All epifluorescence experiments were subsequently analyzed using Image J.

For end-point cell imaging, exposure times were 100ms for each channel with no EM gain set and no ND filter added. For time-lapse biosensor imaging, exposure times were 100 ms for acceptor direct channel (YFP) and 500ms for all other channels (CFP/YFP FRET and CFP), with no EM gain set and no ND filter added. Cells that were too bright (acceptor channel intensity is 3 standard deviations above mean intensity across experiments) or with significant photobleaching prior to drug addition were excluded from analysis.

QUANTIFICATION AND STATISTICAL ANALYSIS

FRET biosensor analysis

Raw fluorescence images were corrected by subtracting the background fluorescence intensity of a cell-free region from the FRET intensities of biosensor-expressing cells. Cyan/yellow FRET ratios were then calculated at each time point (R). For some curves, the resulting time courses were normalized by dividing the FRET ratio at each time point by the basal ratio value at time zero (R/R_0), which was defined as the FRET ratio at the time point immediately preceding drug addition (R_0). Graphs were plotted using GraphPad Prism 10.

Quantification of cellular puncta

For analysis of puncta number, cell images were individually thresholded and underwent particle analysis with circularity and size cutoffs in ImageJ. For the quantification of the number of puncta per cell in Figures 4B and 5B, cells only with sufficient expression of the condensate perturbator were chosen for analysis. In practical terms, with our set up, only cells with TSapphire fluorescence intensity of 1000 (arbitrary units) were included in our analysis.

Statistics and reproducibility

No statistical methods were used to predetermine the sample size. No sample was excluded from data analysis, and no blinding was used. All data were assessed for normality. For normally distributed data, pairwise comparisons were performed using unpaired two-tailed Student's t tests, with Welch's correction for unequal variances used as indicated. Comparisons between three or more groups were performed using ordinary one-way or two-way analysis of variance (ANOVA) as indicated. For data that were not normally distributed, pairwise comparisons were performed using the Mann-Whitney U test, and comparisons between multiple groups were performed using the Kruskal-Wallis test. All data shown are reported as mean ± SEM and error bars in figures represent SEM of biological triplicates unless indicated otherwise. All data were analyzed and plotted using GraphPad Prism 8 including non-linear regression fitting.